




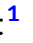







## RESEARCH ARTICLE

# Transcriptomic and morphological maturation of human astrocytes in cerebral organoids

Marloes Verkerke<sup>1</sup>  | Amber Berdenis van Berlekom<sup>1,2</sup>  | Vanessa Donega<sup>3,4</sup>  | Daniëlle Vonk<sup>1</sup>  | Jacqueline A. Sluijs<sup>1</sup>  | Nayab F. Butt<sup>1</sup>  | Lois Kistemaker<sup>1</sup>  | Lot D. de Witte<sup>5</sup>  | R. Jeroen Pasterkamp<sup>1</sup>  | Jinte Middeldorp<sup>6</sup>  | Elly M. Hol<sup>1</sup> 

<sup>1</sup>Department of Translational Neuroscience, UMC Utrecht Brain Center, University Medical Center Utrecht, Utrecht University, Utrecht, The Netherlands

<sup>2</sup>Department of Psychiatry, University Medical Center Utrecht, Brain Center, Utrecht University, Utrecht, The Netherlands

<sup>3</sup>Amsterdam UMC location Vrije Universiteit Amsterdam, Anatomy & Neurosciences, section Clinical Neuroanatomy and Biobanking, Amsterdam, The Netherlands

<sup>4</sup>Amsterdam Neuroscience, Cellular and Molecular Mechanisms, Amsterdam, The Netherlands

<sup>5</sup>Department of Psychiatry, Icahn School of Medicine at Mount Sinai, New York, New York, USA

<sup>6</sup>Department of Neurobiology & Aging, Biomedical Primate Research Centre, Rijswijk, The Netherlands

## Correspondence

Elly M. Hol, Department of Translational Neuroscience, UMC Utrecht Brain Center, University Medical Center Utrecht, Utrecht University, Utrecht, The Netherlands.  
Email: [e.m.hol-2@umcutrecht.nl](mailto:e.m.hol-2@umcutrecht.nl)

## Funding information

Nederlandse Organisatie voor Wetenschappelijk Onderzoek, Grant/Award Numbers: 022.006.001, 024.004.012

## Abstract

Cerebral organoids (CerOrgs) derived from human induced pluripotent stem cells (iPSCs) are a valuable tool to study human astrocytes and their interaction with neurons and microglia. The timeline of astrocyte development and maturation in this model is currently unknown and this limits the value and applicability of the model. Therefore, we generated CerOrgs from three healthy individuals and assessed astrocyte maturation after 5, 11, 19, and 37 weeks in culture. At these four time points, the astrocyte lineage was isolated based on the expression of integrin subunit alpha 6 (ITGA6). Based on the transcriptome of the isolated ITGA6-positive cells, astrocyte development started between 5 and 11 weeks in culture and astrocyte maturation commenced after 11 weeks in culture. After 19 weeks in culture, the ITGA6-positive astrocytes had the highest expression of human mature astrocyte genes, and the predicted functional properties were related to brain homeostasis. After 37 weeks in culture, a subpopulation of ITGA6-negative astrocytes appeared, highlighting the heterogeneity within the astrocytes. The morphology shifted from an elongated progenitor-like morphology to the typical bushy astrocyte morphology. Based on the morphological properties, predicted functional properties, and the similarities with the human mature astrocyte transcriptome, we concluded that ITGA6-positive astrocytes have developed optimally in 19-week-old CerOrgs.

## KEYWORDS

astrocyte, cerebral organoid, iPSC, ITGA6

## 1 | INTRODUCTION

Human induced pluripotent stem cells (iPSCs) have become a valuable tool for the study of astrocytes in health and disease. Especially for research into astrocyte physiology, it is important to use human

in vitro models because human astrocytes differ considerably from rodent astrocytes, such as in morphological complexity, temporal properties of calcium waves, and transcriptomic profile (Li et al., 2021; Oberheim et al., 2009). Additionally, iPSCs can be derived directly from patient's cells which allows for the study of patient-specific disease mechanisms, and this contributes to the clinical applicability of the results. In this study, we differentiated iPSCs into cerebral

Marloes Verkerke and Amber Berdenis van Berlekom contributed equally to this work.

This is an open access article under the terms of the [Creative Commons Attribution](https://creativecommons.org/licenses/by/4.0/) License, which permits use, distribution and reproduction in any medium, provided the original work is properly cited.

© 2023 The Authors. GLIA published by Wiley Periodicals LLC.

organoids (CerOrgs) (Lancaster & Knoblich, 2014; Ormel et al., 2018). CerOrgs are the product of a relatively unguided differentiation process in which only a favorable culture environment for neural differentiation is provided without additional patterning factors. This results in a 3D neural structure with regions reminiscent of different brain areas such as cerebral cortex, hippocampus, and choroid plexus (Lancaster et al., 2013; Renner et al., 2017). An important advantage of this protocol is that it allows for the development of neuroectodermal lineages (neurons, astrocytes, oligodendrocytes) as well as mesodermal lineages (microglia, pericytes) (Matsui et al., 2018; Ormel et al., 2018). Microglia play a crucial role in astrocyte development and maturation. Studies have shown that depletion of microglia results in reduced gliogenesis *in vitro* (Antony et al., 2011; Walton et al., 2006) and microglia-derived nitric oxide enhances astrocyte complexity *in vivo* (Béchéde et al., 2011; MacMicking et al., 1995). Given the intricate interplay between astrocytes and microglia in health and disease, and their engagement with neurons at the synapse, the CerOrgs are a suitable model to study human astrocytes in a 3D environment (Huffels et al., 2022; Matejuk & Ransohoff, 2020; Pasteuning-Vuhman et al., 2021). Therefore, it is important to characterize astrocyte development in CerOrgs in detail to map the maturation of these astrocytes in time and provide a framework for the community for optimal experimental design.

In this study, we first validated the differentiation of CerOrgs from three healthy individuals by bulk RNA sequencing the entire organoid which confirmed the presence of important brain cell types. Next, we determined the molecular profile of astrocytes during their maturation by performing bulk RNA sequencing. Several markers have been identified to isolate astrocytes from brain tissue, such as Hepatic and Glial Cell Adhesion Molecule (HepaCAM) (Zhang et al., 2016) and Solute Carrier Family 1 Member 2 (SLC1A2/GLT1) (Orre et al., 2014; Sun et al., 2017). However, these markers are not always effective to isolate iPSC-derived astrocytes (Barbar et al., 2020). Recently, integrin subunit alpha 6 (ITGA6/CD49f) was identified as a marker for astrocytes in iPSC-derived models and it is also expressed in human post-mortem astrocytes (Barbar et al., 2020; Zhang et al., 2016). ITGA6 belongs to the family of integrins which are cell surface receptors for laminin. These receptors allow for communication between the extracellular matrix and the cytoskeleton (Pérez et al., 2021) and are involved in various processes like cell differentiation, cell adhesion, and the formation of the neurovascular unit (Pérez et al., 2021; Tanigami et al., 2012). Thus, we isolated astrocytes based on ITGA6 expression from CerOrgs after 5, 11, 19, and 37 weeks in culture (WIC) to cover the entire maturation process from progenitor stage to astrocyte maturation. The time points were selected based on previous studies showing that astrocyte development in CerOrgs starts around WIC 12–14 (Dang et al., 2021; Kanton et al., 2019; Renner et al., 2017).

Currently, there is a lack of thorough characterization of the development of astrocytes in this specific model, which hinders the adequate utilization of CerOrgs in human astrocyte research. Therefore, we analyzed the transcriptome of the ITGA6-positive (ITGA6+) and the ITGA6-negative (ITGA6-) cells with bulk RNA

sequencing. As ITGA6 is a relatively new astrocyte marker, we first assessed which cell types were present in the ITGA6+ and ITGA6- fractions. As the ITGA6+ fraction contained the astrocyte lineage, we continued to look *in situ* at the location and morphology of the ITGA6+ in the CerOrgs. The morphology of the ITGA6+ cells evolved from an elongated progenitor-like shape to the typical bushy astrocyte morphology. These morphological properties were linked to biological processes that were predicted based on the transcriptome data. Furthermore, we used a panel of human astrocyte genes to compare the maturation of organoid-derived astrocytes to the maturation process of human astrocytes. The expression of human fetal astrocyte genes declined over time, while the expression of human mature astrocyte genes increased over time in the ITGA6+ astrocytes over time. Finally, we identified an ITGA6-astrocyte population on WIC 37 and addressed astrocyte heterogeneity in the CerOrgs. Based on these findings, we suggest using CerOrgs that are 19 weeks old or older to investigate fully developed astrocytes in the presence of microglia and neurons.

## 2 | METHODS

### 2.1 | Generation of human cerebral organoids

#### 2.1.1 | iPSC line generation and maintenance

The Medical Ethical Committee of the University Medical Center Utrecht granted approval for iPSC line generation. Donors gave written informed consent. Human iPSCs were generated from fibroblasts of 3 healthy individuals and published previously (Harschnitz et al., 2016) (Vieira de Sa et al., in preparation): iPSC 1 (male, 62 years old), iPSC 2 (male, 61 years old), and iPSC 4 (female, 60 years old). Human iPSCs were cultured feeder-free on Geltrex-coated (Thermo Fisher, A1413202) culture dishes in StemFlex medium (Thermo Fisher, A3349401) at 37°C with 5% CO<sub>2</sub>. Once a week, iPSCs were passaged when at 80%–90% confluency. Colonies were detached with 0.5 mM EDTA (Thermo Fisher, 15575020) and transferred to a new dish with additional 5 μM ROCK-inhibitor Y-27632 (Axon Medchem, 1683) for 24 h.

#### 2.1.2 | Cerebral organoid differentiation

The CerOrgs were differentiated as previously described (Ormel et al., 2018), with minor adaptations. The iPSC colonies were detached with 0.5 mM EDTA followed by Accutase (Thermo Fisher, A11105-01) in order to achieve a single cell suspension. The cells were centrifuged at 200 relative centrifugal force (rcf) at room temperature for 4 min and resuspended in HES0 medium (DMEM/F-12 (Thermo Fisher, 11320074), 20% KnockOut Serum Replacement (KOSR; Thermo Fisher, 10828028), 3% Fetal Bovine Serum (FBS; Sigma-Aldrich, F7524), 1% L-glutamine (Thermo Fisher, 25030024), 1% Non-Essential AminoAcids (NEAA; Thermo Fisher, 11140035),

and 0.0007%  $\beta$ -mercaptoethanol (Merck, 805740)) supplemented with 50  $\mu$ M ROCK inhibitor and 4 ng/mL basic Fibroblast Growth Factor (bFGF; Thermo Fisher, AA10155). The single cell suspension was seeded in an Aggrewell 800 microwell plate (StemCell Technologies, 27865) at 3.5 million cells per well on day 0. On day 2, the EBs were manually selected based on size and cellular density. The selected EBs were transferred to an ultra-low attachment 96-well plate (Corning, 3474). On day 4, the ROCK inhibitor and bFGF were withdrawn from the HES0 medium. From day 6 to day 12, the formation of neuroectoderm was facilitated by replacing the medium with Neural Induction Medium (DMEM/F-12, 1% N2 (Thermo Fisher, 17502048), 1% L-Glutamine, 1% NEAA, and 0.5  $\mu$ g/mL heparin (Sigma-Aldrich, H3149-10KU)). On day 13, the CerOrgs were manually selected based on the formation of neuroectoderm and embedded in 30  $\mu$ L matrigel (Corning, 356234). Until day 17, the CerOrgs were cultured in Differentiation Medium without vitamin A (1:1 DMEM/F-12:Neurobasal [Thermo Fisher, 21103049]), 1% L-glutamine, 1% penicillin/streptomycin (P/S; Thermo Fisher, 15140122), 1% B27 without vitamin A (Thermo Fisher, 12587010), 0.5% NEAA, 0.5% N2, 0.025% insulin (Sigma-Aldrich, I9278-5ML), and 0.0003%  $\beta$ -mercaptoethanol). From day 17 onwards, the CerOrgs were cultured in Differentiation Medium with vitamin A (B27 with vitamin A [Thermo Fisher, 17504001]) on a belly dancer (speed 3; IBI Scientific BDRLS0001). Samples for real-time quantitative polymerase chain reaction (qPCR), Western Blot, and immunohistochemistry were taken from 1 differentiation experiment of iPSC 4 and iPSC 1, and from 2 differentiation experiments of iPSC 2. Samples for RNAseq were taken from several batches: three batches of iPSC 1, two batches of iPSC 2, two batches of iPSC 4.

## 2.2 | Bulk RNAseq of cerebral organoids

### 2.2.1 | Fluorescence-activated cell sorting of ITGA6– expressing cells from cerebral organoids

We isolated cells from CerOrgs based on ITGA6 expression according to an earlier published paper (Barbar et al., 2020) with minor adaptations. For each sort, 7 CerOrgs were pooled from 1 iPSC line. First, the CerOrgs were cut into small pieces and dissociated with StemPro Accutase (Thermo Fisher, A1110501) at 37°C on an Incu-Shaker (90 rounds per minute (rpm); Merck, Z763551) for 30 min. We triturated every 10 min to obtain a single-cell suspension. The enzymatic digestion was quenched with DMEM/F12 with 1% FBS and the cell suspension was passed through a 100  $\mu$ m cell strainer. After centrifugation (300 rcf, room temperature, 4 min), the cell pellet was dissolved in FACS buffer (Dulbecco's phosphate-buffered saline (DPBS; Thermo Fisher, 14190169), 0.3% bovine serum albumin (BSA; Sigma-Aldrich, A4503), 12 mM glucose, 2 mM EDTA) and stained with PE rat anti-human ITGA6 antibody (1:50; BD Biosciences, 555736) on ice for 20 min. After centrifugation, the cells were resuspended in fluorescence-activated cell sorting (FACS) buffer and passed through a 70  $\mu$ m cell strainer immediately before sorting. Before sorting, a part

of the cell suspension was set aside and used as total fraction. We used 7AAD (1:50; BD Biosciences, 559925) for dead cell exclusion. The gating strategy was determined based on three control samples: unstained, ITGA6– only stained and 7AAD-only stained. The gates were determined for each iPSC line and time point separately (Figure S1). The cells were sorted on a BD FACSAria™ II (BD Biosciences), using a 100  $\mu$ m nozzle and 20 psi. We collected the ITGA6-positive (ITGA6+) fraction, the ITGA6-negative (ITGA6–) fraction, and the total fraction for bulk RNA sequencing. The total fraction of iPSC 1 on WIC 11 was lost during the sorting procedure and not used for bulk RNA sequencing.

### 2.2.2 | RNA isolation of cerebral organoids for bulk RNAseq

The FACS samples were centrifuged at 12000 rcf for 10 min and the cell pellet was dissolved in 500  $\mu$ L QIAzol Lysis Reagent (Qiagen, 217004). The RNA was isolated with the miRNeasy mini kit (Qiagen, 217004) according to the manufacturer's protocol including removal of genomic DNA. The RNA was dissolved in MilliQ and stored at –80°C until further processing. The RNA concentration was measured with the Nanodrop 2000 Spectrophotometer (Thermo Fisher, ND-2000) and the RNA quality was analyzed with the RNA 6000 Pico Kit (Agilent, 5067–1513) using the Bioanalyzer 2100 (Agilent, G2939BA) (Table S1).

### 2.2.3 | Bulk RNAseq of cerebral organoids

The samples were sequenced at Single Cell Discoveries, Utrecht, The Netherlands (Muraro et al., 2016). The complementary DNA (cDNA) libraries were prepared according to the CEL-Seq2 protocol (Hashimshony et al., 2012). In brief, a custom-made primer for each sample was added to the RNA, which was denatured at 70°C for 2 min and then immediately cooled down. The mRNA was reverse transcribed into cDNA, purified using clean-up beads (Thermo Fisher), and then transcribed in vitro to obtain amplified RNA using the MegaScript kit. The amplified RNA was purified using Agencourt RNAClean XP (RNase free) beads (Beckman Coulter) and subsequently fragmented with fragmentation buffer. After purification with RNA clean XP beads, the quality of the RNA was determined with the RNA 6000 Pico Kit using the Bioanalyzer 2100. Subsequently, the amplified RNA was reverse transcribed, amplified by PCR, and labeled with a 4 base pairs (bp) unique molecular identifier (UMI) which was added to the primer. The libraries were sequenced using the Illumina NextSeq 500 platform with paired-end sequencing (75 bp) at a sequencing depth of 10 million reads per sample. The raw RNAseq reads were aligned to the human genome (Homo Sapiens GRCh38 Refseq) using the Burrows-Wheeler Aligner (BWA) (Li & Durbin, 2009). Duplicate reads and reads that mapped equally well to multiple locations were discarded. Read counts were normalized by using the median of ratios method from the DESeq2 pipeline version 1.35.0 in R studio version

4.1.0 (Table S2). Differential gene expression was analyzed with DESeq2. Genes were considered differentially expressed with an adjusted  $p$ -value smaller than .01 ( $p_{\text{adj}} < 0.01$ ) (Table S3a).

## 2.2.4 | Downstream analysis of bulk RNAseq

We loaded the lists of differentially expressed genes in the EnrichR web-based tool (<http://amp.pharm.mssm.edu/Enrich/>) using the gene ontology (GO) Biological Process 2021 (Table S3b) (Chen et al., 2013; Kuleshov et al., 2016; Xie et al., 2021). Graphs were created in Graphpad Prism (version 9.5.0).

For the heatmaps in Figure 3, we used a list of 200 genes that were identified as characteristic for human fetal and mature astrocytes by (Sloan et al., 2017). Of these 200 genes, 8 fetal genes (*HIST1H2AI*, *HIST1H2AK*, *HIST1H2BF*, *HIST2H2AA3*, *LOC100144602*, *RP1-177G6.2*, *RPL13AP6*, *SCARNA27*) and 4 mature genes (*AGXT2L1*, *HEPN1*, *LOC653513*, *BRP44L*) were not expressed in the ITGA6+ cells and therefore excluded from the analysis. For the remaining 188 genes, the Z score was calculated for every iPSC line separately with the next formula:  $z = (x - \mu) / \sigma$ , where  $x$  is the normalized counts on a time point,  $\mu$  is the mean of all time points, and  $\sigma$  is the standard deviation. Heatmaps were created with Morpheus (<https://software.broadinstitute.org/morpheus>) and hierarchical clustering of the genes was performed with the one minus Pearson correlation. The 92 fetal genes separated in seven clusters and the 96 mature genes separated in five clusters (Table S4). For the largest three fetal and two mature gene clusters, the median Z-score of each gene and the median Z-score of the entire cluster were visualized in a line graph.

## 2.3 | Validation on entire cerebral organoids

### 2.3.1 | qPCR on cerebral organoids

The CerOrgs were collected individually in 500  $\mu\text{L}$  QIAzol Lysis Reagent and lysed with the Ultra TurraxHomogenizer (IKA, 0003737000). The RNA isolation was done similar to the FACS samples. The QuantiTect Reverse Transcription Kit (Qiagen, 205311) was used to convert RNA into complementary DNA. The reverse transcription reaction was started with 0.5  $\mu\text{g}$  RNA or 6  $\mu\text{L}$  RNA when the RNA concentration was too low. The cDNA samples were stored at  $-20^{\circ}\text{C}$  until further use.

For each qPCR reaction, the input was 5 ng cDNA with 5  $\mu\text{L}$  FastStart Universal SYBR green Master (Sigma-Aldrich, 4913914001), 1  $\mu\text{L}$  primer mix (forward and reverse primers, 5 pmol/ $\mu\text{L}$ ; see Table S5), and MilliQ up to a total volume of 11  $\mu\text{L}$ . All primers were designed with Primer BLAST (NCBI). The qPCR reaction was performed with the QuantStudio 6 Flex Real-Time PCR System (Applied Biosystems) with the following cycling conditions: 2 min at  $50^{\circ}\text{C}$ ; 10 min at  $95^{\circ}\text{C}$ ; 15 s at  $95^{\circ}\text{C}$ ; 1 min at  $60^{\circ}\text{C}$ ; and 15 s at  $95^{\circ}\text{C}$  for 40 cycles. Specificity of the primers was

checked with melt curves. Undetermined values were replaced by the lowest cycle threshold (CT) value of 40. Absolute expression levels were calculated ( $2^{-\text{CT}}$ ) and the expression of genes of interest was normalized to the geomean expression of reference genes *GAPDH* and *SDHA2* as determined by NormFinder (Andersen et al., 2004).

### 2.3.2 | Western blot on cerebral organoids

Single CerOrgs were collected in 100  $\mu\text{L}$  suspension buffer (0.1 M NaCl, 0.01 M Tris-HCl, 0.001 M EDTA, pH 7.6) with complete EDTA-free protease inhibitor cocktail (Roche, 11697498001) and phosphatase inhibitor cocktail (Sigma-Aldrich, P5726). After dissociation with the Ultra Turrax, 100  $\mu\text{L}$  of 2x SDS (sodium dodecyl sulfate) buffer (100 mM Tris, 4% SDS, 20% glycerol, 0.2 M DL-Dithiothreitol (Sigma-Aldrich, D9779), pH 6.8) was added and samples were heated at  $95^{\circ}\text{C}$  for 5 min. The DNA was broken down by pushing samples through a 25G needle several times. For visibility of the sample, Bromophenol Blue (Merck, 34725-61-6) was added. The total protein samples were loaded on a 10% SDS gel and separated by electrophoresis. Proteins were transferred to a 0.45  $\mu\text{m}$  pore-size nitrocellulose membrane (GE Healthcare, A20485269) using a wet/tank transfer blotting system (Biorad, 170390). The membranes were blocked with supermix (25 mM Tris, 77 mM NaCl, 69 mM gelatin, 0.25% Triton X-100, pH 7.4) at room temperature for 10 min. The primary antibody was incubated at  $4^{\circ}\text{C}$  overnight and the secondary antibody was incubated at room temperature for 1 h (Table S5). After washing with phosphate buffered saline (PBS), the membrane was imaged on the Odyssey CLX LI-COR scanner. Overnight, the membrane was restained for the reference protein GAPDH. The signal of the target protein was normalized to the signal of GAPDH.

### 2.3.3 | Immunohistochemistry of cerebral organoids

The CerOrgs were collected and washed with PBS before fixation in 4% Paraformaldehyde (PFA) Aqueous Solution (Fisher Scientific, 50-980-487) at  $4^{\circ}\text{C}$  overnight. The CerOrgs were washed 3 times with PBS and incubated in 30% sucrose in PBS at  $4^{\circ}\text{C}$  overnight. The CerOrgs were snap-frozen on dry ice in Tissue-Tek<sup>®</sup> O.C.T. Compound (Sakura Finetek Europe, 4583) and sliced on a cryostat in 20  $\mu\text{m}$  sections. Slides were stored at  $-20^{\circ}\text{C}$  until further use. The sections were washed with PBS + 0.05% Tween and blocked at room temperature with blocking buffer for 1 h (PBS, 1% Triton-X, 3% BSA, 10% donkey serum (Abcam, ab7475)). The primary antibody was incubated at  $4^{\circ}\text{C}$  overnight and the secondary antibody was incubated at room temperature for 1 h (Table S5). The slides were washed in PBS and mounted with glass coverslips using FluorSave (CalBioChem, 345789). Imaging was performed on a Zeiss AxioScope A1 microscope with the EC Plan-Neofluar 40x/0.75 M27 objective and the AxioCAM MRm camera with Software Axiovision (version 4.8.2.0).



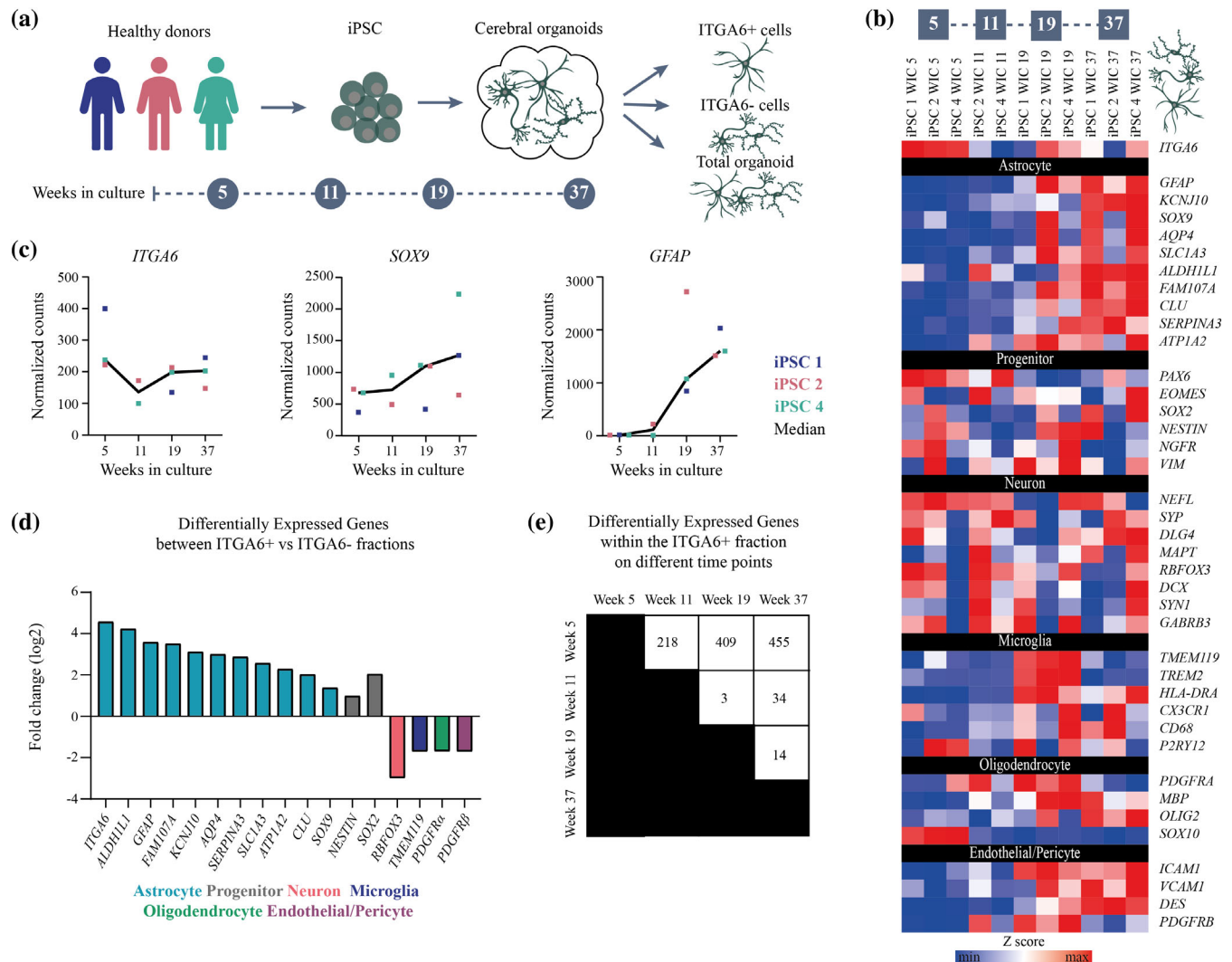
## 3 | RESULTS

## 3.1 | ITGA6-positive fraction contains cells from the astrocyte lineage

The CerOrgs were made from iPSCs of three healthy donors (Ormel et al., 2018). To focus specifically on astrocytes, we explored different markers to isolate astrocytes from CerOrgs. Classical astrocyte markers SLC1A2 and HepaCAM were not effective for the isolation of a substantial number of astrocytes from CerOrgs (data not shown),

despite their common use for rodent astrocyte isolation (Orre et al., 2014; Zhang et al., 2016). Therefore, we used the recently identified astrocyte marker ITGA6 (Barbar et al., 2020), which was abundantly expressed in CerOrgs (Figure S2a). The ITGA6+ and ITGA6- cells were isolated from CerOrgs that had been in culture for 5, 11, 19, or 37 weeks (weeks in culture = WIC). Bulk RNA sequencing was performed on both the ITGA6+ and ITGA6- fractions in addition to the total CerOrg on the four-time points (Figure 1a).

We first checked the development of major brain cell types, namely astrocytes, progenitors, neurons, microglia, endothelial cells,



**FIGURE 1** Characterization of the ITGA6-positive cells in the cerebral organoids. (a) Schematic overview of the experimental set up. Cerebral organoids were made from iPSCs of 3 healthy donors (iPSC 1, iPSC 2, iPSC 4), and the ITGA6+, ITGA6-, and total fraction were bulk RNA sequenced after 5, 11, 19, and 37 weeks in culture (WIC). (b) Relative gene expression of selected genes in the total fraction. Every column represents one iPSC line on a specific time point. Within every iPSC line, the relative expression over time was calculated as Z score for every gene. Blue indicates the lowest expression of a gene and red the highest expression. (c) Normalized counts of *ITGA6*, *SOX9*, and *GFAP* in the total fraction. Symbols represent the number of normalized counts for each iPSC line, with in blue iPSC 1, in pink iPSC 2, and in green iPSC 4. The black line represents the median of the 3 iPSC lines. (d) The log<sub>2</sub> fold change of the significantly differentially expressed genes with an adjusted *p*-value of < 0.01 between the ITGA6+ and ITGA6- fraction. A positive log<sub>2</sub> fold change reflects a higher gene expression in the ITGA6+ cells, while a negative log<sub>2</sub> fold change reflects a higher gene expression in the ITGA6- cells. The colors indicate the cell type in which a specific gene is expressed. (e) The number of significant differentially expressed genes with an adjusted *p*-value < 0.01 in the ITGA6+ cells between different time points. iPSC, induced pluripotent stem cell; ITGA6, integrin subunit 6 alpha; WIC, weeks in culture.

pericytes, and oligodendrocytes in the total CerOrg based on a panel of marker genes (Figure 1b). *ITGA6* was expressed at all-time points with the highest expression on WIC 5 (Figure 1b,c). The selected astrocyte genes were generally lowly expressed on the early time points (WIC 5 and 11) and increased in expression on the later time points (WIC 19 and 37) (Figure 1b). The expression of most astrocyte genes, such as *GFAP*, steeply increased between WIC 11 and 19 (Figure 1c). The expression of the transcription factor *SOX9*, which is crucial for gliogenesis, was already expressed at WIC 5 and 11, but increased further between WIC 11 and 19 (Figure 1c). In the total organoid, the expression patterns of *GFAP* and *SOX9* as determined with bulk RNA sequencing (Figure 1b,c) corresponded with the pattern of mRNA expression as determined with qPCR and with the pattern of protein expression as determined with Western Blot (Figure S2b). The selected progenitor genes were expressed relatively constant over time, only *PAX6* expression decreased at later time points. The selected neuronal genes were also expressed relatively constant over time, indicating that neuronal differentiation had already started before WIC 5. Finally, the expression of most of the selected microglia, oligodendrocyte, and endothelial/pericyte genes peaked at the later time points. The transcription factor *SOX10*, expressed in oligodendrocyte progenitor cells, showed higher expression in early time points. However, the level of gene expression varied significantly between these cell-type-specific genes (Figure S2c).

Next, we validated the cell types in the *ITGA6*<sup>+</sup> and in the *ITGA6*<sup>-</sup> fractions (Figure 1d). The expression of *ITGA6* was significantly higher ( $p_{\text{adj}} = 7.78\text{E}-34$ ) in the *ITGA6*<sup>+</sup> than in the *ITGA6*<sup>-</sup> cells indicating a successful isolation procedure. The selected astrocyte marker genes were all significantly increased in the *ITGA6*<sup>+</sup> cells, such as *GFAP* ( $p_{\text{adj}} = 8.64\text{E}-05$ ), *FAM107A* ( $p_{\text{adj}} = 8.53\text{E}-12$ ), and *CLU* ( $p_{\text{adj}} = 8.26\text{E}-10$ ). In contrast, the selected genes for cell types other than astrocytes were significantly increased in the *ITGA6*<sup>-</sup> cells, such as the neuronal gene *RBFOX3* ( $p_{\text{adj}} = 7.54\text{E}-07$ ) and the microglia gene *TMEM119* ( $p_{\text{adj}} = 3.19\text{E}-03$ ). However, the progenitor genes *SOX2* ( $p_{\text{adj}} = 8.82\text{E}-05$ ) and *NESTIN* ( $p_{\text{adj}} = 2.25\text{E}-05$ ) were also significantly higher in the *ITGA6*<sup>+</sup> cells.

Thus, the population of *ITGA6*<sup>+</sup> cells consisted of the entire astrocyte lineage, from progenitors to astrocytes. To assess the development of the astrocyte lineage over time, we compared the transcriptome of the *ITGA6*<sup>+</sup> cells between time points. The largest number of differentially expressed genes (DEG) in the *ITGA6*<sup>+</sup> fraction was between WIC 5 and WIC 37 ( $n = 455$  with  $p_{\text{adj}} < 0.01$ ) (Figure 1e). Between consecutive time points, the largest change in gene expression in the *ITGA6*<sup>+</sup> cells was from WIC 5 to WIC 11 with 218 DEG (with  $p_{\text{adj}} < 0.01$ ). For example, the expression of *WNT3A*, which inhibits gliogenesis (Bem et al., 2019), was significantly decreased ( $p_{\text{adj}} = 4.63\text{E}-04$ ) while the expression of *TNC*, which is a fetal astrocyte gene (Fu et al., 2021), was significantly increased ( $p_{\text{adj}} = 4.02\text{E}-04$ ) between WIC 5 and WIC 11. Between WIC 11 and WIC 19, there were only three DEG and the most significant DEG was the mature astrocyte marker *PMP2* ( $p_{\text{adj}} = 1.38\text{E}-09$ ). This indicated that the differentiation of progenitors to fetal astrocytes commenced between WIC 5 and WIC 11 and that the astrocytes matured

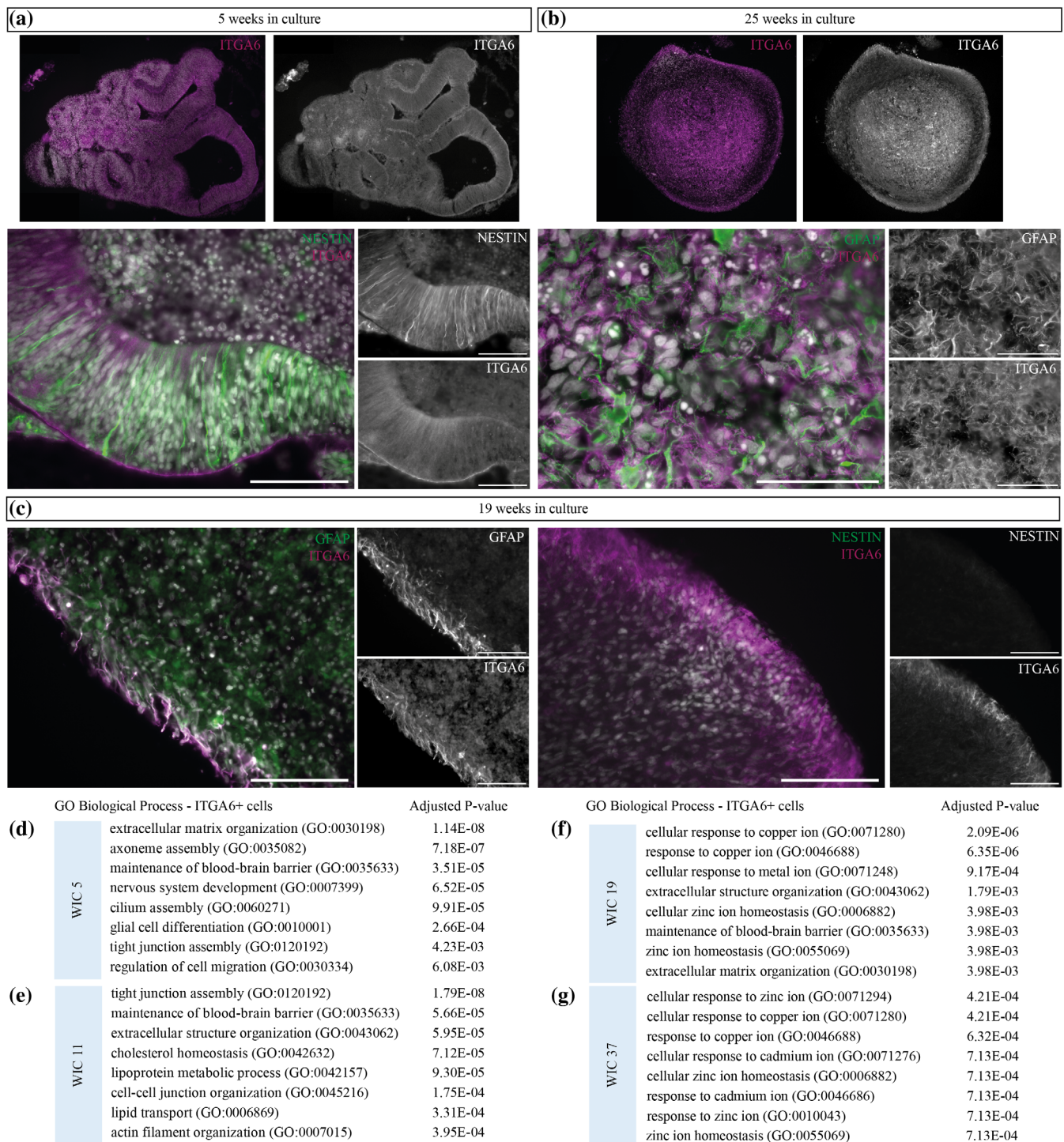
from WIC 11 onwards. Next, we checked whether this timeline of differentiation and maturation in the *ITGA6*<sup>+</sup> cells was reflected in morphological changes and predicted functional changes.

### 3.2 | Mature *ITGA6*<sup>+</sup> cells are characterized by a typical astrocyte morphology and express genes involved in typical astrocyte processes

The morphology of the *ITGA6*<sup>+</sup> cells changed significantly over time and corresponded with the changes in transcriptome that were observed. On WIC 5, the *ITGA6* protein was present in the progenitor zones of the CerOrgs with an accumulation in the outer edges of the zone (Figure 2a). In these progenitor zones, the *ITGA6*<sup>+</sup> cells also expressed the progenitor marker *NESTIN* and morphologically resembled the elongated shape of human progenitors (Figure 2a). On WIC 25, which is in the middle of the presumed astrocyte maturation period between WIC 11 and WIC 37, the localization of the *ITGA6* protein shifted to the outer edges of the CerOrg (Figure 2b). The expression of *ITGA6* co-localized with *GFAP* and these *ITGA6*<sup>+</sup> *GFAP*<sup>+</sup> cells had numerous processes reminiscent of a typical bushy astrocyte shape (Figure 2b). On WIC 19, we identified *ITGA6*<sup>+</sup> cells that co-expressed *GFAP* but did not express *NESTIN* (Figure 2c).

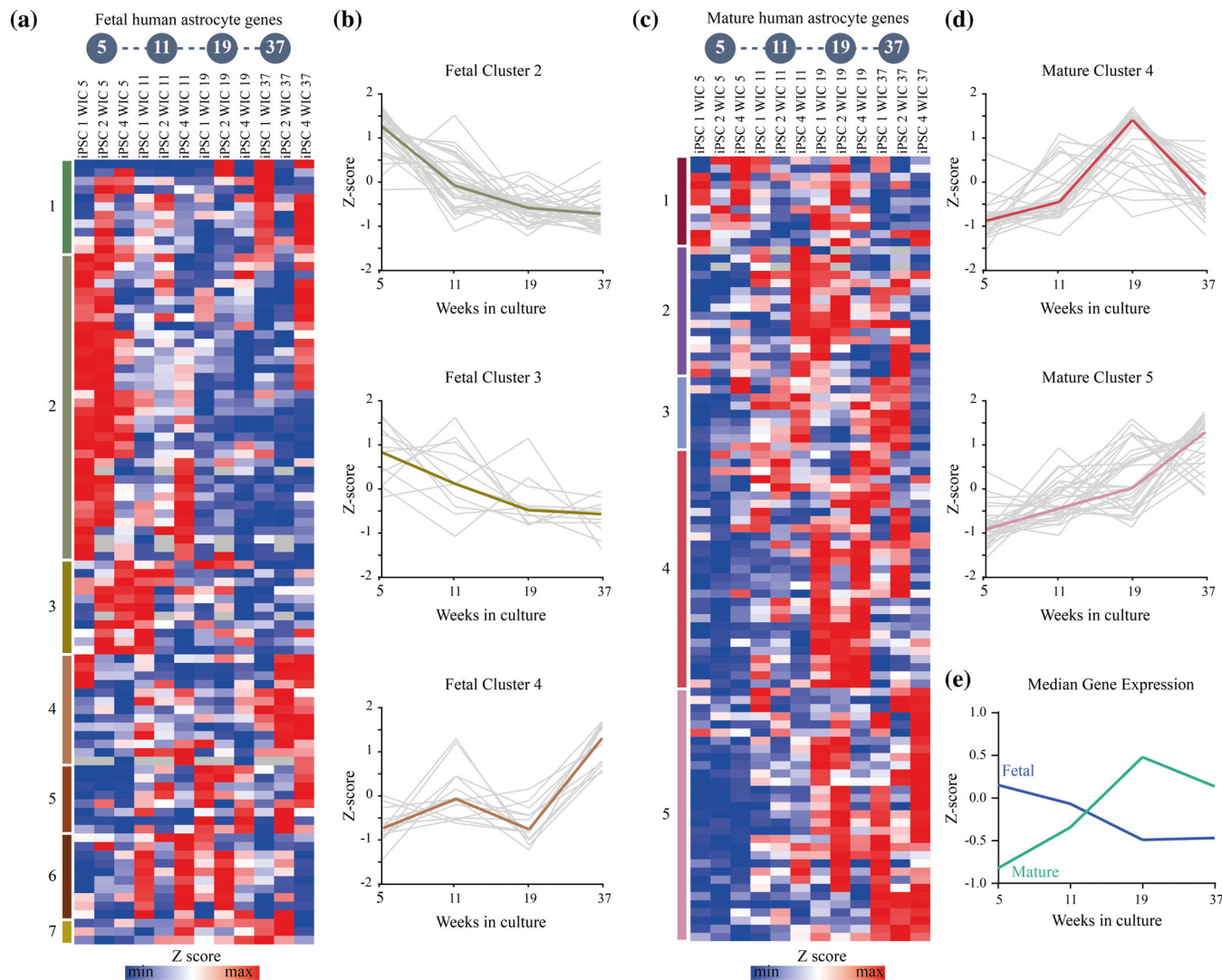
The changes in transcriptome and morphology have most likely an effect on the functional properties of the *ITGA6*<sup>+</sup> cells. Therefore, we performed gene ontology (GO) analysis on the DEG between the *ITGA6*<sup>+</sup> and *ITGA6*<sup>-</sup> on every time point and looked at the Biological Processes to predict the functional properties of *ITGA6*<sup>+</sup> cells. On WIC 5, the GO terms represented progenitor-related processes such as *nervous system development* ( $p_{\text{adj}} = 6.52\text{E}-05$ ), *cilium assembly* ( $p_{\text{adj}} = 9.91\text{E}-05$ ), *glial cell differentiation* ( $p_{\text{adj}} = 2.66\text{E}-04$ ), and *regulation of cell migration* ( $p_{\text{adj}} = 6.08\text{E}-03$ ) (Figure 2d). On WIC 11, several lipid-related GO processes were detected, such as *cholesterol homeostasis* ( $p_{\text{adj}} = 7.12\text{E}-05$ ), *lipoprotein metabolic process* ( $p_{\text{adj}} = 9.30\text{E}-05$ ), and *lipid transport* ( $p_{\text{adj}} = 3.31\text{E}-04$ ) (Figure 2e). On WIC 19 and WIC 37, the majority of GO processes were related to ion homeostasis, such as *cellular response to copper ion* (WIC 19  $p_{\text{adj}} = 2.09\text{E}-06$ ; WIC 37  $p_{\text{adj}} = 4.21\text{E}-04$ ) and *cellular zinc homeostasis* (WIC 19  $p_{\text{adj}} = 3.98\text{E}-03$ ; WIC 37  $p_{\text{adj}} = 7.13\text{E}-04$ ) (Figure 2f,g). These ion-related GO processes were a reflection of a variety of genes on WIC 19, but were mainly driven by only four *Metallothionein (MT)* genes on WIC 37. Finally, it was remarkable that the GO process *maintenance of the blood-brain barrier* was enriched in the *ITGA6*<sup>+</sup> cells on WIC 5 ( $p_{\text{adj}} = 3.51\text{E}-05$ ), WIC 11 ( $p_{\text{adj}} = 5.66\text{E}-05$ ), and WIC 19 ( $p_{\text{adj}} = 35.66\text{E}-05$ ) even though there is no blood-brain barrier present in the CerOrgs. The genes in this GO process are related to tight junctions (*CLDN3*, *OCLN*) and gap junctions (*GJA1*). The GO analysis on the DEG enriched in the *ITGA6*<sup>-</sup> cells revealed primarily neuronal processes on all the time points (Figure S2d).

In conclusion, the *ITGA6*<sup>+</sup> cells on WIC 5 corresponded to progenitors with an elongated morphology that were predicted to perform functions related to brain development. The *ITGA6*<sup>+</sup> cells from WIC 19 onwards corresponded to astrocytes with a bushy



**FIGURE 2** Morphology and predicted functional properties of ITGA6+ cells. (a) Representative image of localization of cells that expressed ITGA6 (magenta) in cerebral organoids that had been in culture for 5 weeks. These cells also expressed NESTIN (green). Nuclei are visualized in white. Scale bar, 100  $\mu$ m. (b) Representative image of cells that expressed ITGA6 (magenta) in cerebral organoids that had been in culture for 25 weeks. These cells also expressed GFAP (green). Nuclei are visualized in white. Scale bar, 50  $\mu$ m. (c) Representative image of cells that expressed ITGA6 (magenta) in cerebral organoids after 19 weeks in culture. These ITGA6+ cells did express GFAP (green, left), but did not express NESTIN (green, right). Scale bar, 100  $\mu$ m. (d–g) The significant GO Biological Process terms based on the significantly differentially expressed genes ( $p_{adj} < 0.01$ ) enriched in the ITGA6+ compared to the ITGA6– cells after 5 weeks in culture (d), 11 weeks in culture (e), 19 weeks in culture (f), and 37 weeks in culture (g). GO, gene ontology; ITGA6, integrin subunit 6 alpha; WIC, weeks in culture.





**FIGURE 3** Expression of fetal and mature astrocyte genes in the ITGA6+ cells. (a) Heatmap showing the expression of 92 fetal human astrocyte genes in the ITGA6+ cells over time. The Z-score was calculated for every gene within an iPSC line and color coded with blue meaning the lowest expression and red the highest. The genes were clustered based on one minus Pearson correlation which resulted in 7 clusters. (b) The median expression of the three largest fetal clusters is depicted. For every gene in a cluster, the median expression of the 3 iPSC lines combined is depicted as the gray lines. For each cluster, the median expression of all genes in that cluster is depicted in the colored line. (c) Heatmap showing the expression of 96 mature human astrocyte genes in the ITGA6+ cells over time. The Z-score was calculated for every gene within an iPSC line and color coded with blue meaning the lowest expression and red the highest. The genes were clustered based on one minus Pearson correlation and 5 main clusters were identified. (d) The median expression of the two largest mature clusters is depicted. For every gene in a cluster, the median expression of the 3 iPSC lines combined is depicted as the gray lines. For each cluster, the median expression of all genes in that cluster is depicted in the colored line. (e) The median expression of the 92 fetal genes (blue line) and 96 mature genes (turquoise line) in the ITGA6+ cells over time.

morphology that were predicted to perform functions related to lipid transport, ion homeostasis, and the blood–brain barrier in accordance with known astrocyte functions/reflecting mature astrocyte functions.

### 3.3 | The transcriptome of ITGA6+ astrocytes on WIC 19 resembles the transcriptome of human mature astrocytes

Next, we set out to compare human astrocytes from CerOrgs to human postmortem astrocytes. For this analysis, we used a panel of

100 fetal and 100 mature astrocyte genes that were identified by Sloan et al. (2017), based on the comparison between human astrocytes isolated from fetuses (17–20 gestational weeks) and from adults (8–63 years old) (Zhang et al., 2016). Of these 200 human astrocyte genes, 8 fetal genes and 4 mature genes were not expressed in the ITGA6+ astrocytes and were excluded from the analysis (Table S4). By performing a correlation analysis, the fetal genes separated in 7 clusters with 3 major clusters, namely cluster 2 ( $n = 36$ ), cluster 3 ( $n = 11$ ), and cluster 4 ( $n = 13$ ) (Figure 3a,b; Table S4). The expression of the fetal genes in cluster 2 and 3 was decreased over time with peak expression on WIC 5. In contrast, the expression of the fetal

genes in cluster 4 was increased over time with a peak expression on WIC 37. The mature genes separated in five clusters with three smaller clusters (cluster 1  $n = 11$ ; cluster 2  $n = 16$ ; cluster 3 = 9) and 2 large clusters (cluster 4  $n = 29$ ; cluster 5  $n = 31$ ) (Figure 3c,d; Table S4). Cluster 4 of the mature genes showed an increase in expression until WIC 19 and a decrease in expression on WIC 37. The expression of the mature genes in cluster 5 was increased over time with a peak expression on WIC 37. Overall, the median gene expression of all fetal genes showed a decrease over time, while the mature genes showed an increase over time (Figure 3e). The lowest expression of fetal astrocytes genes and the highest expression of mature astrocytes genes in the *ITGA6*<sup>+</sup> astrocytes was at WIC 19. Interestingly, we observed a slight decrease in expression of mature astrocyte genes in the *ITGA6*<sup>+</sup> astrocytes between WIC 19 and WIC 37. To identify the cause of this decrease, we zoomed-in on the *ITGA6*<sup>+</sup> and *ITGA6*<sup>-</sup> cells at these two time points.

### 3.4 | Two major astrocyte populations arise in cerebral organoids of 37 weeks old

Both on WIC 19 and WIC 37, the expression of *ITGA6* was specific for the *ITGA6*<sup>+</sup> cells compared to the *ITGA6*<sup>-</sup> cells (WIC 19:  $p_{\text{adj}} = 1.20\text{E}-08$ ; WIC 37:  $p_{\text{adj}} = 6.12\text{E}-10$ ) (Figure S3), which further confirmed the successful sorting procedure. However, the number of DEG between the *ITGA6*<sup>+</sup> and *ITGA6*<sup>-</sup> cells was much lower on WIC 37 ( $n = 143$  with  $p_{\text{adj}} < 0.01$ ) compared to WIC 19 ( $n = 550$  with  $p_{\text{adj}} < 0.01$ ). This raised the question whether an astrocyte subpopulation existed in the *ITGA6*<sup>-</sup> fraction on WIC 37, potentially leading to fewer DEG. In the *ITGA6*<sup>-</sup> cells, we checked the expression of the panel of 10 astrocytes genes that we had used to identify the *ITGA6*<sup>+</sup> cells as astrocytes in Figure 1d. On WIC 19, almost all 10 astrocyte genes were specifically expressed in the *ITGA6*<sup>+</sup> cells, except *ALDH1L1* (Figure 4; Figure S3). On WIC 37, only *ITGA6* and *FAM107A* were still specific for the *ITGA6*<sup>+</sup> cells, while the other astrocyte genes were also expressed in the *ITGA6*<sup>-</sup> cells (Figure 4; Figure S3).

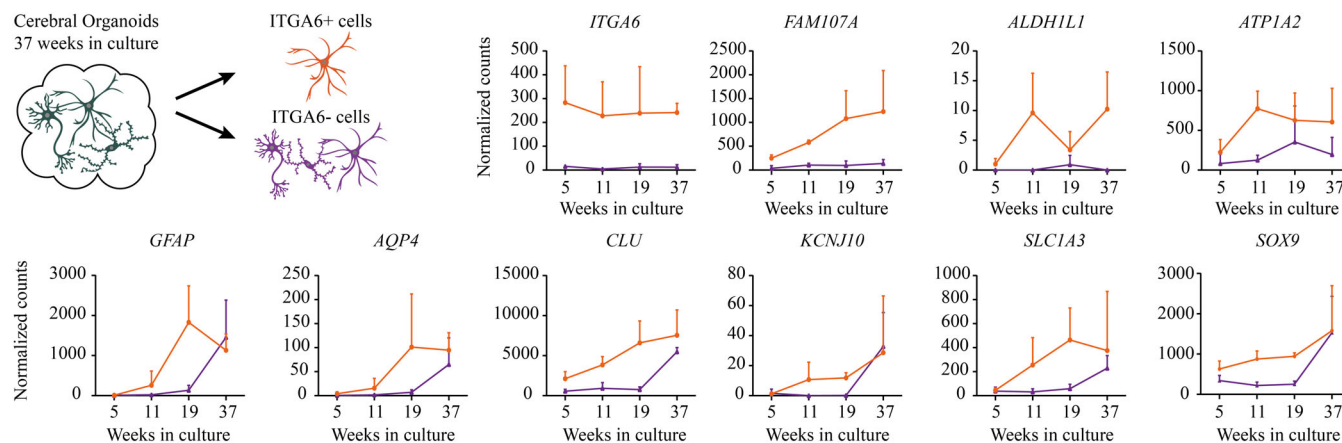
Hence, we concluded that a sub population of astrocytes arose between WIC 19 and WIC 37 in the CerOrgs that could not be isolated based on *ITGA6* expression.

## 4 | DISCUSSION

### 4.1 | Summary of results

Human iPSC-derived CerOrgs are a valuable model to study the interaction between neurons, microglia, and astrocytes in a 3D environment (Ormel et al., 2018; Renner et al., 2017). However, to adequately use CerOrgs in human astrocyte research, the development of astrocytes in this specific model needs to be thoroughly characterized which is currently lacking. In this study, we have assessed astrocyte development and maturation in CerOrgs along an extensive timeline from WIC 5 up to WIC 37. The CerOrgs were derived from three healthy human iPSC lines to ensure a robust outcome that is not donor specific. The development of brain cells in our CerOrgs closely resembled the timeline observed in human brain development. In CerOrgs, neurons were generated before astrocytes started to develop on WIC 11. This transition from neurogenesis to gliogenesis is a well-documented phenomenon occurring in the latter half of fetal brain development (Holst et al., 2019; Miller & Gauthier, 2007). To focus on the development of the astrocyte lineage in the CerOrgs, we isolated this lineage based on *ITGA6* expression and the changing transcriptome was analyzed over time with bulk RNAseq.

On WIC 5, the *ITGA6*<sup>+</sup> cells were located in the progenitor zones of the CerOrgs. The *ITGA6*<sup>+</sup> cells co-localized with NESTIN and had an elongated morphology. With the GO analysis, the predicted functions of the *ITGA6*<sup>+</sup> were all related to nervous system development. For example, cilium assembly was one of the significant GO terms and the formation of primary cilia is crucial for proper cortical development (Zaidi et al., 2022). Additionally, the expression of the panel of human fetal astrocyte genes peaked in the *ITGA6*<sup>+</sup> cells on WIC 5. On WIC 11 and WIC 19, the *ITGA6*<sup>+</sup> cells were maturing and the



**FIGURE 4** Two subpopulations of astrocytes in 37-week-old cerebral organoids. The expression of 10 astrocytes genes in the *ITGA6*<sup>+</sup> cells (orange) and the *ITGA6*<sup>-</sup> cells (purple). Expression levels are depicted as normalized counts. Lines are the means with standard deviation.



expression of the panel of mature astrocyte genes increased until the peak expression on WIC 19. At the same time, the expression of human fetal astrocyte genes decreased until the lowest expression on WIC 19. The GO analysis revealed typical astrocyte functions in lipid metabolism and ion homeostasis. Additionally, the morphology of the ITGA6+ cells had evolved from an elongated shape to a bushy astrocyte shape on WIC 25. Interestingly, a subpopulation of astrocytes appeared on WIC 37 that did not express *ITGA6*, suggesting heterogeneity among astrocytes in the CerOrgs model.

Taken together, CerOrgs that have been in culture for 19 weeks contained ITGA6+ astrocytes with a transcriptome and morphology resembling human mature astrocytes. Additionally, the CerOrgs do not only contain developed astrocytes at this time point, but also other neural cell types including microglia.

## 4.2 | Considerations for comparing organoid-derived astrocytes to postmortem astrocytes

To investigate the astrocyte maturation process in CerOrgs, we used a panel of fetal and mature genes that was identified based on the transcriptome of postmortem astrocytes. However, this comparison between organoid-derived astrocytes and postmortem astrocytes should be done with consideration. Different data sets of human postmortem astrocytes have used different markers and different brain regions to isolate astrocytes. The human postmortem astrocytes used in this study were isolated based on HepaCAM expression from the temporal cortex, while the organoid-derived astrocytes were isolated based on *ITGA6* expression. In our CerOrgs, HepaCAM was not expressed and could thus not be used to isolate the astrocytes. The expression of HepaCAM seems to be highly dependent on the organoid differentiation protocol as some groups have been able to use HepaCAM to isolate from organoids (Sloan et al., 2017) while others reported the same absence of HepaCAM expression as in our CerOrgs (Barbar et al., 2020). With the well-known heterogeneity of astrocytes in the human brain and the variety in organoid differentiation protocols, it should be considered that a comparison between different astrocyte data sets could reflect a comparison between different subtypes (Bayraktar et al., 2020; Ben Haim & Rowitch, 2016; Dang et al., 2021; Holst et al., 2019).

## 4.3 | Astrocyte heterogeneity in cerebral organoids

We observed astrocyte heterogeneity in CerOrgs at WIC 37. At this time point, two astrocyte subpopulations could be distinguished based on the expression of *ITGA6*. The ITGA6- astrocytes were present in the fraction that also contained neurons and other cell types. This made it challenging to characterize this specific subpopulation of ITGA6- astrocytes. The ITGA6+ astrocytes were characterized by the expression of several *MT* genes (*MT2A*, *MT1F*, *MT1X*, *MT1E*). *MT*s are polypeptides that maintain the low intracellular concentration of

metals and additionally regulate transcription and translation of inflammatory and apoptosis-related genes (Sharma & Ebadi, 2014). In the brain, *MT1* and *MT2* are predominantly expressed by astrocytes (Penkowa et al., 1999; Waller et al., 2018). With normal aging, human astrocytes upregulate the *MT* genes as adaptive response to oxidative stress (Li et al., 2014; Lu et al., 2004; Verkerke et al., 2021). In pathological aging conditions such as Alzheimer's Disease, the expression of *MT*s in astrocytes is significantly increased compared to age-matched controls. This is a coping mechanism against amyloid beta induced oxidative stress and cell death (Kim et al., 2012; Zambenedetti et al., 1998). The expression of the *MT* genes in the ITGA6+ astrocytes followed the same pattern as genes like *GFAP* and *AQP4*. This suggests that the upregulation of the *MT* genes is most likely the result of an increasingly mature astrocyte population rather than an adaptive response to oxidative stress. However, we cannot exclude the possibility that the necrotic core inside the CerOrgs stimulates the expression of the *MT* genes in astrocytes.

## 4.4 | Functional properties of astrocytes in cerebral organoids

The functional properties that we ascribed to the ITGA6+ astrocyte in the CerOrgs were predicted based on the transcriptomic profile. Functional characterization of astrocytes in CerOrgs is still lacking. There are, to our knowledge, no studies that assess astrocyte functioning over time in this specific CerOrg model. Some studies have done functional assays on isolated astrocytes from other organoid models (Dezonne et al., 2017; Pasca et al., 2015; Sloan et al., 2017). However, these studies used more guided differentiation protocols and the organoids lacked microglia. The crosstalk between microglia and astrocytes is crucial for the regulation of brain homeostasis. For example, a main function of microglia is pruning of excessive synapses thereby shaping the neuronal network (Schafer et al., 2012). In turn, synaptic activity influences the maturation of astrocytes (Morel et al., 2014). Therefore, it is plausible that the presence of microglia in the CerOrg model influences the functioning of both neurons and astrocytes. How the presence of microglia in our CerOrgs influences the functioning of astrocytes has yet to be determined.

## 4.5 | Power of iPSC-based studies

In this study, we have used iPSC lines derived from three healthy individuals. Despite the known heterogeneity present in organoid cultures, we found that the timing of astrocyte development and maturation in CerOrgs was consistent between the three iPSC lines. Other studies have found the same result in different organoid models and this indicates that specific developmental cues are intrinsically present in the organoid cultures, regardless of iPSC line (Pasca et al., 2015; Voss et al., 2023). While comparable studies only use one iPSC line, we realize that results derived from three iPSC lines might still not be representable for the entire population (Dang et al., 2021; Kanton et al., 2019; Quadrato et al., 2017;



Renner et al., 2017). In the field of organoid research, the number of iPSC lines used per study is often determined empirically (Revah et al., 2022; Voss et al., 2023). In animal studies, it is common to perform a power analysis based on effect size to prevent underpowered studies. It should become common practice to also perform these analyses for iPSC-based studies to increase the applicability of the results (Brunner et al., 2022). Using this approach, we can fully utilize the potential of iPSC-based studies to reveal mechanisms that apply to entire populations as well as those unique to individuals.

## 5 | CONCLUSION

In this study, we isolated the astrocyte lineage from CerOrgs on WIC 5, 11, 19, and 37 based on ITGA6 expression. The change in morphology of the ITGA6<sup>+</sup> cells from elongated to bushy correlated with the changing transcriptome and both indicated a maturation process from progenitor to astrocyte. The expression of mature human astrocyte genes peaked at WIC 19 in the ITGA6<sup>+</sup> astrocytes. On WIC 37, we identified an ITGA6<sup>-</sup> subpopulation of astrocytes which emphasized the presence of astrocyte heterogeneity in CerOrgs. Based on morphological properties, predicted functional properties, and similarities with the human mature astrocyte transcriptome, we concluded that ITGA6<sup>+</sup> astrocytes have developed optimally in CerOrgs on WIC 19. Therefore, we recommend to use 19-week-old or older CerOrgs to study developed astrocytes in the presence of microglia and neurons.

### AUTHOR CONTRIBUTIONS

Marloes Verkerke and Amber Berdenis van Berlekom designed the study under supervision of Elly M. Hol and Lot D. de Witte. Marloes Verkerke and Amber Berdenis van Berlekom performed the study in collaboration with Daniëlle Vonk, Jacqueline A. Sluijs, Nayab F. Butt, and Lois Kistemaker. Vanessa Donega performed the processing and analysis of the bulk RNA sequencing data. Marloes Verkerke analyzed the data and wrote the manuscript, including the revisions. Lot D. de Witte, R. Jeroen Pasterkamp, Jinte Middeldorp, and Elly M. Hol supervised the study and collaboratively edited and co-wrote the paper.

### ACKNOWLEDGMENTS

This work was supported by the Dutch Research Council (NWO) Graduate Program (022.006.001) (MV) and by the NWO Gravitation Program BRAINSCAPES: A Roadmap from Neurogenetics to Neurobiology (024.004.012) (EMH).

### CONFLICT OF INTEREST STATEMENT

The authors have no conflicts of interest to declare that are relevant to the content of this article.

### DATA AVAILABILITY STATEMENT

The bulk RNA sequencing data are available at the NCBI Gene Expression Omnibus (GEO) repository (GSE244778). Other data are available

upon request from the corresponding author: [e.m.hol-2@umcutrecht.nl](mailto:e.m.hol-2@umcutrecht.nl).

### ORCID

Marloes Verkerke <https://orcid.org/0000-0001-9397-9876>

Amber Berdenis van Berlekom <https://orcid.org/0000-0002-7546-0250>

Vanessa Donega <https://orcid.org/0000-0002-3152-2675>

Lois Kistemaker <https://orcid.org/0000-0002-7114-1252>

Lot D. de Witte <https://orcid.org/0000-0002-7235-9958>

R. Jeroen Pasterkamp <https://orcid.org/0000-0003-1631-6440>

Jinte Middeldorp <https://orcid.org/0000-0002-9198-8020>

Elly M. Hol <https://orcid.org/0000-0001-5604-2603>

### REFERENCES

- Andersen, C. L., Jensen, J. L., & Ørntoft, T. F. (2004). Normalization of real-time quantitative reverse transcription-PCR data: A model-based variance estimation approach to identify genes suited for normalization, applied to bladder and colon cancer data sets. *Cancer Research*, 64(15), 5245–5250. <https://doi.org/10.1158/0008-5472.CAN-04-0496>
- Antony, J. M., Paquin, A., Nutt, S. L., Kaplan, D. R., & Miller, F. D. (2011). Endogenous microglia regulate development of embryonic cortical precursor cells. *Journal of Neuroscience Research*, 89(3), 286–298. <https://doi.org/10.1002/jnr.22533>
- Barbar, L., Jain, T., Zimmer, M., Kruglikov, I., Sadick, J. S., Wang, M., Kalpana, K., Rose, I. V. L., Burstein, S. R., Rusielewicz, T., Nijssure, M., Guttenplan, K. A., di Domenico, A., Croft, G., Zhang, B., Nobuta, H., Hébert, J. M., Liddelov, S. A., & Fossati, V. (2020). CD49f is a novel marker of functional and reactive human iPSC-derived astrocytes. *Neuron*, 107(3), 436–453.e12. <https://doi.org/10.1016/j.neuron.2020.05.014>
- Bayraktar, O. A., Bartels, T., Holmqvist, S., Kleshchevnikov, V., Martirosyan, A., Polioudakis, D., Ben Haim, L., Young, A. M. H., Batiuk, M. Y., Prakash, K., Brown, A., Roberts, K., Paredes, M. F., Kawaguchi, R., Stockley, J. H., Sabour, K., Chang, S. M., Huang, E., Hutchinson, P., ... Rowitch, D. H. (2020). Astrocyte layers in the mammalian cerebral cortex revealed by a single-cell in situ transcriptomic map. *Nature Neuroscience*, 23, 500–509. <https://doi.org/10.1038/s41593-020-0602-1>
- Béchéde, C., Pascual, O., Triller, A., & Bessis, A. (2011). Nitric oxide regulates astrocyte maturation in the hippocampus: Involvement of NOS2. *Molecular and Cellular Neuroscience*, 46(4), 762–769. <https://doi.org/10.1016/j.mcn.2011.02.009>
- Bem, J., Brożko, N., Chakraborty, C., Lipiec, M. A., Koziński, K., Nagalski, A., Szewczyk, Ł. M., & Wiśniewska, M. B. (2019). Wnt/ $\beta$ -catenin signaling in brain development and mental disorders: Keeping TCF7L2 in mind. *FEBS Letters*, 593(13), 1654–1674. <https://doi.org/10.1002/1873-3468.13502>
- Ben Haim, L., & Rowitch, D. H. (2016). Functional diversity of astrocytes in neural circuit regulation. *Nature Reviews Neuroscience*, 18(1), 31–41. <https://doi.org/10.1038/nrn.2016.159>
- Brunner, J. W., Lammertse, H. C. A., van Berkel, A., Koopmans, F., Li, K. W., Smit, A. B., Toonen, R. F., Verhage, M., & van der Sluis, S. (2022). Power and optimal study design in iPSC-based brain disease modelling. *Molecular Psychiatry*, 28, 1545–1556. <https://doi.org/10.1038/s41380-022-01866-3>
- Chen, E. Y., Tan, C. M., Kou, Y., Duan, Q., Wang, Z., Meirelles, G. V., Clark, N. R., & Ma'ayan, A. (2013). Enrichr: Interactive and collaborative HTML5 gene list enrichment analysis tool. *BMC Bioinformatics*, 14, 128. <https://doi.org/10.1186/1471-2105-14-128>
- Dang, J., Tiwari, S. K., Agrawal, K., Hui, H., Qin, Y., & Rana, T. M. (2021). Glial cell diversity and methamphetamine-induced neuroinflammation

- in human cerebral organoids. *Molecular Psychiatry*, 26(4), 1194–1207. <https://doi.org/10.1038/s41380-020-0676-x>
- Dezonne, R. S., Sartore, R. C., Nascimento, J. M., Saia-Cereda, V. M., Romão, L. F., Alves-Leon, S. V., de Souza, J. M., Martins-de-Souza, D., Rehen, S. K., & Gomes, F. C. (2017). Derivation of functional human astrocytes from cerebral organoids. *Scientific Reports*, 7, 1–14. <https://doi.org/10.1038/srep45091>
- Fu, Y., Yang, M., Yu, H., Wang, Y., Wu, X., Yong, J., Mao, Y., Cui, Y., Fan, X., Wen, L., Qiao, J., & Tang, F. (2021). Heterogeneity of glial progenitor cells during the neurogenesis-to-gliogenesis switch in the developing human cerebral cortex. *Cell Reports*, 34(9), 108788. <https://doi.org/10.1016/j.celrep.2021.108788>
- Harschnitz, O., van den Berg, L. H., Johansen, L. E., Jansen, M. D., Kling, S., Vieira de Sá, R., Vlam, L., van Rheenen, W., Karst, H., Wierenga, C. J., Pasterkamp, R. J., & van der Pol, W. L. (2016). Autoantibody pathogenicity in a multifocal motor neuropathy induced pluripotent stem cell-derived model. *Annals of Neurology*, 80(1), 71–88. <https://doi.org/10.1002/ana.24680>
- Hashimshony, T., Wagner, F., Sher, N., & Yanai, I. (2012). CEL-seq: Single-cell RNA-seq by multiplexed linear amplification. *Cell Reports*, 2(3), 666–673. <https://doi.org/10.1016/j.celrep.2012.08.003>
- Holst, C. B., Bröchner, C. B., Vitting-Seerup, K., & Møllgård, K. (2019). Astroglialogenesis in human fetal brain: Complex spatiotemporal immunoreactivity patterns of GFAP, S100, AQP4 and YKL-40. *Journal of Anatomy*, 235(3), 590–615. <https://doi.org/10.1111/joa.12948>
- Huffels, C. F. M., Middeldorp, J., & Hol, E. M. (2022). Aβ pathology and neuron–glia interactions: A synaptocentric view. *Neurochemical Research*, 48, 1026–1046. <https://doi.org/10.1007/s11064-022-03699-6>
- Kanton, S., Boyle, M. J., He, Z., Santel, M., Weigert, A., Sanchís-Calleja, F., Guijjarro, P., Sidow, L., Fleck, J. S., Han, D., Qian, Z., Heide, M., Huttner, W. B., Khaitovich, P., Pääbo, S., Treutlein, B., & Camp, J. G. (2019). Organoid single-cell genomic atlas uncovers human-specific features of brain development. *Nature*, 574, 418–422.
- Kim, J. H., Nam, Y. P., Jeon, S. M., Han, H. S., & Suk, K. (2012). Amyloid neurotoxicity is attenuated by metallothionein: Dual mechanisms at work. *Journal of Neurochemistry*, 121(5), 751–762. <https://doi.org/10.1111/j.1471-4159.2012.07725.x>
- Kuleshov, M. V., Jones, M. R., Rouillard, A. D., Fernandez, N. F., Duan, Q., Wang, Z., Koplev, S., Jenkins, S. L., Jagodnik, K. M., Lachmann, A., McDermott, M. G., Monteiro, C. D., Gundersen, G. W., & Ma'ayan, A. (2016). Enrichr: A comprehensive gene set enrichment analysis web server 2016 update. *Nucleic Acids Research*, 44(W1), W90–W97. <https://doi.org/10.1093/nar/gkw377>
- Lancaster, M. A., & Knoblich, J. A. (2014). Generation of cerebral organoids from human pluripotent stem cells. *Nature Protocols*, 9(10), 2329–2340. <https://doi.org/10.1038/nprot.2014.158>
- Lancaster, M. A., Renner, M., Martin, C. A., Wenzel, D., Bicknell, L. S., Hurles, M. E., Homfray, T., Penninger, J. M., Jackson, A. P., & Knoblich, J. A. (2013). Cerebral organoids model human brain development and microcephaly. *Nature*, 501(7467), 373–379. <https://doi.org/10.1038/nature12517>
- Li, H., & Durbin, R. (2009). Fast and accurate short read alignment with burrows-wheeler transform. *Bioinformatics*, 25(14), 1754–1760. <https://doi.org/10.1093/bioinformatics/btp324>
- Li, J., Pan, L., Pembroke, W. G., Rexach, J. E., Godoy, M. I., Condro, M. C., Alvarado, A. G., Harteni, M., Chen, Y. W., Stiles, L., Chen, A. Y., Wanner, I. B., Yang, X., Goldman, S. A., Geschwind, D. H., Kornblum, H. I., & Zhang, Y. (2021). Conservation and divergence of vulnerability and responses to stressors between human and mouse astrocytes. *Nature Communications*, 12(1), 1–20. <https://doi.org/10.1038/s41467-021-24232-3>
- Li, M. D., Burns, T. C., Morgan, A. A., & Khatri, P. (2014). Integrated multi-cohort transcriptional meta-analysis of neurodegenerative diseases. *Acta Neuropathologica Communications*, 2, 93.
- Lu, T., Pan, Y., Kao, S. Y., Li, C., Kohane, I., Chan, J., & Yankner, B. A. (2004). Gene regulation and DNA damage in the ageing human brain. *Nature*, 429(6994), 883–891. <https://doi.org/10.1038/nature02661>
- MacMicking, J. D., Nathan, C., Hom, G., Chartrain, N., Fletcher, D. S., Trumbauer, M., Stevens, K., Xie, Q. W., Sokol, K., Hutchinson, N., Chen, H., & Mudgett, J. S. (1995). Altered responses to bacterial infection and endotoxic shock in mice lacking inducible nitric oxide synthase. *Cell*, 81(4), 641–650. [https://doi.org/10.1016/0092-8674\(95\)90085-3](https://doi.org/10.1016/0092-8674(95)90085-3)
- Matejuk, A., & Ransohoff, R. M. (2020). Crosstalk between astrocytes and microglia: An overview. *Frontiers in Immunology*, 11(July), 1–11. <https://doi.org/10.3389/fimmu.2020.01416>
- Matsui, T. K., Matsubayashi, M., Sakaguchi, Y. M., Hayashi, R. K., Zheng, C., Sugie, K., Hasegawa, M., Nakagawa, T., & Mori, E. (2018). Six-month cultured cerebral organoids from human ES cells contain matured neural cells. *Neuroscience Letters*, 670(February), 75–82. <https://doi.org/10.1016/j.neulet.2018.01.040>
- Miller, F. D., & Gauthier, A. S. (2007). Timing is everything: Making neurons versus glia in the developing cortex. *Neuron*, 54(3), 357–369. <https://doi.org/10.1016/j.neuron.2007.04.019>
- Morel, L., Higashimori, H., Tolman, M., & Yang, Y. (2014). VGluT1+ neuronal glutamatergic signaling regulates postnatal developmental maturation of cortical protoplasmic astroglia. *Journal of Neuroscience*, 34(33), 10950–10962. <https://doi.org/10.1523/JNEUROSCI.1167-14.2014>
- Muraro, M. J., Dharmadhikari, G., Grün, D., Groen, N., Dielen, T., Jansen, E., van Gurp, L., Engelse, M. A., Carlotti, F., de Koning, E. J. P., & van Oudenaarden, A. (2016). A single-cell transcriptome atlas of the human pancreas. *Cell Systems*, 3(4), 385–394.e3. <https://doi.org/10.1016/j.cels.2016.09.002>
- Oberheim, N. A., Takano, T., Han, X., He, W., Lin, J. H. C., Wang, F., Xu, Q., Wyatt, J. D., Pilcher, W., Ojemann, J. G., Ransom, B. R., Goldman, S. A., & Nedergaard, M. (2009). Uniquely hominid features of adult human astrocytes. *Journal of Neuroscience*, 29(10), 3276–3287. <https://doi.org/10.1523/JNEUROSCI.4707-08.2009>
- Ormel, P. R., Vieira de Sá, R., van Bodegraven, E. J., Karst, H., Harschnitz, O., Sneeboer, M. A. M., Johansen, L. E., van Dijk, R. E., Scheefhals, N., Berdenis van Berlekom, A., Ribes Martínez, E., Kling, S., MacGillavry, H. D., van den Berg, L. H., Kahn, R. S., Hol, E. M., de Witte, L. D., & Pasterkamp, R. J. (2018). Microglia innately develop within cerebral organoids. *Nature Communications*, 9(1), 4167. <https://doi.org/10.1038/s41467-018-06684-2>
- Orre, M., Kamphuis, W., Osborn, L. M., Melief, J., Kooijman, L., Huitinga, I., Klooster, J., Bossers, K., & Hol, E. M. (2014). Acute isolation and transcriptome characterization of cortical astrocytes and microglia from young and aged mice. *Neurobiology of Aging*, 35(1), 1–14. <https://doi.org/10.1016/j.neurobiolaging.2013.07.008>
- Pasca, A. M., Sloan, S. A., Clarke, L. E., Tian, Y., Makinson, C. D., Huber, N., Kim, C. H., Park, J.-Y., O'Rourke, N. A., Nguyen, K. D., Smith, S. J., Huguenard, J. R., Geschwind, D. H., Barres, B. A., & Pasca, S. P. (2015). Functional cortical neurons and astrocytes from human pluripotent stem cells in 3D culture. *Nature Methods*, 12(7), 671–678. <https://doi.org/10.1038/nmeth.3415>
- Pasteuning-Vuhman, S., de Jongh, R., Timmers, A., & Pasterkamp, R. J. (2021). Towards advanced iPSC-based drug development for neurodegenerative disease. *Trends in Molecular Medicine*, 27(3), 263–279. <https://doi.org/10.1016/j.molmed.2020.09.013>
- Penkowa, M., Nielsen, H., Hidalgo, J., Bernth, N., & Moos, T. (1999). Distribution of metallothionein I + II and vesicular zinc in the developing central nervous system: Correlative study in the rat. *Journal of Comparative Neurology*, 412(2), 303–318. [https://doi.org/10.1002/\(SICI\)1096-9861\(19990920\)412:2<303::AID-CNE9>3.0.CO;2-G](https://doi.org/10.1002/(SICI)1096-9861(19990920)412:2<303::AID-CNE9>3.0.CO;2-G)
- Pérez, L. A., Rashid, A., Combs, J. D., Schneider, P., Rodríguez, A., Salaita, K., & Leyton, L. (2021). An outside-in switch in integrin signaling caused by chemical and mechanical signals in reactive astrocytes. *Frontiers in Cell and Developmental Biology*, 9(August), 1–14. <https://doi.org/10.3389/fcell.2021.712627>



- Quadrato, G., Nguyen, T., Macosko, E. Z., Sherwood, J. L., Min Yang, S., Berger, D. R., Maria, N., Scholvin, J., Goldman, M., Kinney, J. P., Boyden, E. S., Lichtman, J. W., Williams, Z. M., McCarroll, S. A., & Arlotta, P. (2017). Cell diversity and network dynamics in photosensitive human brain organoids. *Nature*, *545*(7652), 48–53. <https://doi.org/10.1038/nature22047>
- Renner, M., Lancaster, M. A., Bian, S., Choi, H., Ku, T., Peer, A., Chung, K., & Knoblich, J. A. (2017). Self-organized developmental patterning and differentiation in cerebral organoids. *The EMBO Journal*, *36*(10), 1316–1329. <https://doi.org/10.15252/embj.201694700>
- Revah, O., Gore, F., Kelley, K. W., Andersen, J., Sakai, N., Chen, X., Li, M. Y., Birey, F., Yang, X., Saw, N. L., Baker, S. W., Amin, N. D., Kulkarni, S., Mudipalli, R., Cui, B., Nishino, S., Grant, G. A., Knowles, J. K., Shamloo, M., ... Paşca, S. P. (2022). Maturation and circuit integration of transplanted human cortical organoids. *Nature*, *610*, 319–326. <https://doi.org/10.1038/s41586-022-05277-w>
- Schafer, D. P., Lehrman, E. K., Kautzman, A. G., Koyama, R., Mardinly, A. R., Yamasaki, R., Ransohoff, R. M., Greenberg, M. E., Barres, B. A., & Stevens, B. (2012). Microglia sculpt postnatal neural circuits in an activity and complement-dependent manner. *Neuron*, *74*, 691–705. <https://doi.org/10.1016/j.neuron.2012.03.026>
- Sharma, S., & Ebadi, M. (2014). Significance of metallothioneins in aging brain. *Neurochemistry International*, *65*(1), 40–48. <https://doi.org/10.1016/j.neuint.2013.12.009>
- Sloan, S. A., Darmanis, S., Huber, N., Khan, T. A., Birey, F., Caneda, C., Reimer, R., Quake, S. R., Barres, B. A., & Paşca, S. P. (2017). Human astrocyte maturation captured in 3D cerebral cortical spheroids derived from pluripotent stem cells. *Neuron*, *95*(4), 779–790.e6. <https://doi.org/10.1016/j.neuron.2017.07.035>
- Sun, W., Cornwell, A., Li, J., Peng, S., Osorio, M. J., Aalling, N., Wang, S., Benraiss, A., Lou, N., Goldman, S. A., & Nedergaard, M. (2017). SOX9 is an astrocyte-specific nuclear marker in the adult brain outside the neurogenic regions. *Journal of Neuroscience*, *37*(17), 4493–4507. <https://doi.org/10.1523/JNEUROSCI.3199-16.2017>
- Tanigami, H., Okamoto, T., Yasue, Y., & Shimaoka, M. (2012). Astroglial integrins in the development and regulation of neurovascular units. *Pain Research and Treatment*, *2012*, 1–10. <https://doi.org/10.1155/2012/964652>
- Verkerke, M., Hol, E. M., & Middeldorp, J. (2021). Physiological and pathological ageing of astrocytes in the human brain. *Neurochemical Research*, *46*, 2662–2675. <https://doi.org/10.1007/s11064-021-03256-7>
- Voss, A. J., Lanjewar, S. N., Sampson, M. M., King, A., Hill, E. J., Sing, A., Sojka, C., Bhatia, T. N., Spangle, J. M., & Sloan, S. A. (2023). Identification of ligand–receptor pairs that drive human astrocyte development. *Nature Neuroscience*, *26*(August), 1339–1351. <https://doi.org/10.1038/s41593-023-01375-8>
- Waller, R., Murphy, M., Garwood, C. J., Jennings, L., Heath, P. R., Chambers, A., Matthews, F. E., Brayne, C., Ince, P. G., Wharton, S. B., Simpson, J. E., & Cognitive Function and Ageing Neuropathology Study Group. (2018). Metallothionein-I/II expression associates with the astrocyte DNA damage response and not Alzheimer-type pathology in the aging brain. *Glia*, *66*(11), 2316–2323. <https://doi.org/10.1002/glia.23465>
- Walton, N. M., Sutter, B. M., Laywell, E. D., Levkoff, L. H., Kearns, S. M., Marshall, G. P., II, Scheffler, B., & Steindler, D. A. (2006). Microglia Instruct Subventricular Zone Neurogenesis. *Glia*, *54*, 815–825. <https://doi.org/10.1002/glia>
- Xie, Z., Bailey, A., Kuleshov, M. V., Clarke, D. J. B., Evangelista, J. E., Jenkins, S. L., Lachmann, A., Wojciechowicz, M. L., Kropiwnicki, E., Jagodnik, K. M., Jeon, M., & Ma'ayan, A. (2021). Gene set knowledge discovery with Enrichr. *Current Protocols*, *1*(3), e90. <https://doi.org/10.1002/cpz1.90>
- Zaidi, D., Chinnappa, K., & Francis, F. (2022). Primary cilia influence progenitor function during cortical development. *Cell*, *11*(18), 213–214. <https://doi.org/10.1016/j.neuron.2004.10.002>
- Zambenedetti, P., Giordano, R., & Zatta, P. (1998). Metallothioneins are highly expressed in astrocytes and microcapillaries in Alzheimer's disease. *Journal of Chemical Neuroanatomy*, *15*(1), 21–26. [https://doi.org/10.1016/S0891-0618\(98\)00024-6](https://doi.org/10.1016/S0891-0618(98)00024-6)
- Zhang, Y., Sloan, S. A., Clarke, L. E., Caneda, C., Plaza, C. A., Blumenthal, P. D., Vogel, H., Steinberg, G. K., Edwards, M. S. B., Li, G., Duncan, J. A., III, Cheshier, S. H., Shuer, L. M., Chang, E. F., Grant, G. A., Gephart, M. G. H., & Barres, B. A. (2016). Purification and characterization of progenitor and mature human astrocytes reveals transcriptional and functional differences with mouse. *Neuron*, *89*(1), 37–53. <https://doi.org/10.1016/j.neuron.2015.11.013>

## SUPPORTING INFORMATION

Additional supporting information can be found online in the Supporting Information section at the end of this article.

**How to cite this article:** Verkerke, M., Berdenis van Berlekom, A., Donega, V., Vonk, D., Sluijs, J. A., Butt, N. F., Kistemaker, L., de Witte, L. D., Pasterkamp, R. J., Middeldorp, J., & Hol, E. M. (2024). Transcriptomic and morphological maturation of human astrocytes in cerebral organoids. *Glia*, *72*(2), 362–374. <https://doi.org/10.1002/glia.24479>